THE JOURNAL OF PHYSICAL CHEMISTRY C

Article

Cite This: J. Phys. Chem. C 2018, 122, 19385−19394

pubs.acs.org/JPCC

Influence of 4 and 4′ Substituents on $Ru^{III/II}$ Bipyridyl Self-Exchange Electron Transfer Across Nanocrystalline TiO_2 Surfaces

Tyler C. Motley, Matthew D. Brady, and Gerald J. Meyer*

Department of Chemistry, University of North Carolina at Chapel Hill, Chapel Hill, North Carolina 27599, United States

Supporting Information

ABSTRACT: Lateral self-exchange electron transfer across oxide surfaces is important to many solar energy capture and conversion schemes. Substituent effects on lateral $Ru^{III/II}$ self-exchange electron transfer were studied using a series of Ru^{II} polypyridyl compounds of the type $[Ru(R_2bpy)_2(P)]^{2+}$, where P is 2,2′-bipyridyl-4,4′-diphosphonic acid and R_2bpy was a 4,4′-substituted-2,2′-bipyridine with six different R groups: $-OCH_3$, $-C(CH_3)_3$, $-CH_3$, −H, −Br, and $-CF_3$. These functional groups were chosen mainly for their electron-withdrawing or -donating ability. Chronoabsorptometry was used to probe the apparent diffusion coefficient, D_{CA}, that was proportional to the self-exchange rate constants, and these values were found to be between 2.8×10^{-11} and 7.9×10^{-9} cm^2/s. The measured D_{CA} values showed no correlation with the electron-withdrawing or -donating ability of the functional groups, but were instead correlated with the steric size of the substituents that also influenced the saturation surface coverage and thus the intermolecular distance. With some assumptions to estimate the intermolecular distance, the self-exchange rates were found to possess an exponential dependence with the distance, $\beta = 1.2 \pm 0.2$ $Å^{-1}$. Independent tests of the were carried out by varying the surface coverages from which $\beta = 1.18 \pm 0.09$ $Å^{-1}$ was found. The results indicate that the substituent's steric size is the dominant factor that controls lateral $Ru^{III/II}$ self-exchange electron-transfer rates at these interfaces.

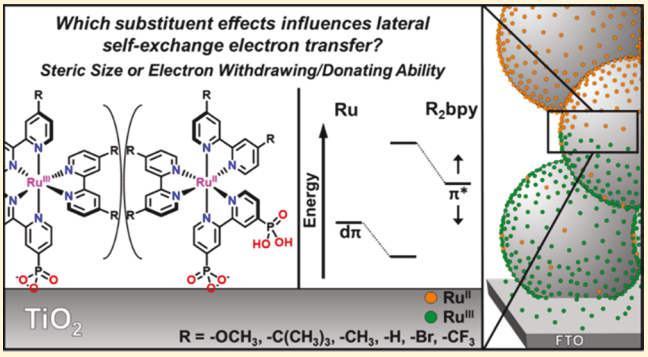

INTRODUCTION

Lateral electron transfer, commonly referred to as hole hopping, between surface-immobilized, redox active compounds at semiconductor interfaces provides a means to laterally transport charge without a loss of free energy and has emerged as an important process in molecular approaches to solar energy conversion. Recent reports revealed that after dye-sensitized excited-state electron injection into TiO_2, the rate at which the oxidizing equivalent was translated away from the injection site by lateral self-exchange was directly correlated to charge recombination with the injected electron.[1−3] Moia and co-workers have recently reported an operational dye-sensitized solar cell that utilized hole hopping to translate the oxidizing equivalent to the counter electrodes rather than the traditional iodide redox mediators. This approach led to sustained electrical power generation with notably large open circuit voltages.[4,5] Furthermore, lateral electron transfer was shown to be integral to the accumulation of multiple redox equivalents onto a catalytic site.[6−8] Therefore, control of lateral electron transfer at semiconductor interfaces is an important goal. Here, we expand upon a previous report[9] using a homologous series of Ru^{II} polypyridyl compounds to determine whether the electron-withdrawing/-donating ability of substituents on a 4,4′-substituted-2,2′-bipyridine ligand influence the lateral self-exchange electron-transfer rates at the TiO_2 interface.

Even though the formal $Ru^{III/II}$ reduction potentials lie within the forbidden bandgap, it is well established that surface-anchored Ru^{II} polypyridyl compounds anchored to the mesoporous nanocrystalline TiO_2 thin films commonly used in dye-sensitized solar cells can be quantitatively oxidized with application of a sufficiently positive potential.[10−12] The key requirement for complete oxidation is that the surface coverage be above a minimum value, termed a percolation threshold, which is typically 50−60% of the saturation surface coverage.[9,11−13] The accepted mechanism, depicted in Scheme 1, invokes initial electron transfer to the fluorine-doped tin oxide (FTO) transparent conductive oxide from nearby molecules followed by self-exchange electron transfer through the mesoporous thin film.[9−11,13−17] As time progresses, the diffusion layer, sometimes referred to in these films as the oxidation front, moves through the film until it reaches the outer edges and the film is completely oxidized. This mechanism has been invoked for numerous classes of redox active compounds on oxide surfaces.[9,11,12,14,15]

Self-exchange electron transfer between Ru^{II} polypyridyl compounds in fluid solution and on the surface of metal oxides has been previously modeled with Marcus theory for

Received: June 1, 2018
Revised: July 19, 2018
Published: August 21, 2018

DOI: 10.1021/acs.jpcc.8b05281
J. Phys. Chem. C 2018, 122, 19385−19394

Scheme 1. Simplistic Depiction of the Time Evolution of the Complete Film Oxidation during a Chronoabsorptometry (CA) Experiment

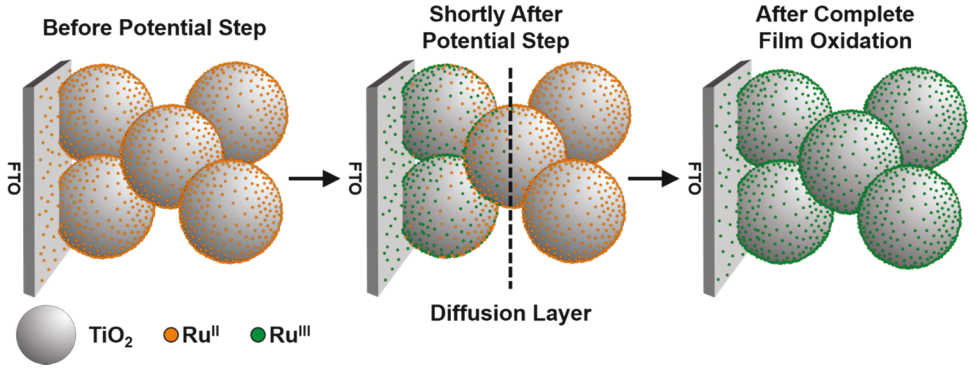

nonadiabatic electron transfer.[9,18] The Marcus equation for self-exchange ($\Delta G^\circ = 0$) is given by eq 1, where k_R is the rate constant for electron transfer, H_{DA} is the intermolecular electronic coupling matrix element between electron donor (Ru^{II}) and electron acceptor (Ru^{III}), k_B is the Boltzmann constant, $\hbar$ is the reduced Planck constant, T is the absolute temperature, and λ is the total reorganization energy with inner- (λ_I) and outer-sphere (λ_O) components. At constant λ and T, the rate constant is expected to depend on H_{DA} that often decreases exponentially with distance as described by eq 2, where δ is the intermolecular distance between the donor and acceptor, β is the attenuation factor, and H^O_{DA} is the electronic coupling at van der Waals separation, δ_O.[19−22]

$$k_R = \left(\frac{2\pi}{\hbar}\right)\left(\frac{|H_{DA}|^2}{\sqrt{4\pi\lambda k_B T}}\right) e^{(-\lambda/4k_B T)} \quad (1)$$

$$H_{DA} = H^O_{DA}\, e^{-(\beta/2)(\delta-\delta_O)} \quad (2)$$

Recently, a homologous series of three $[Ru(R_2bpy)_2(dcb)]^{2+}$ compounds, where R_2bpy was a 4,4′-substituted-2,2′-bipyridine and dcb was 2,2′-bipyridyl-4,4′-dicarboxylic acid, was reported where the steric bulk of the substituent in the 4 and 4′ positions of R_2bpy was systematically increased from −H, $-CH_3$, and $-C(CH_3)_3$ to determine if the addition of insulating side groups would alter the $Ru^{III/II}$ self-exchange rate constants by increasing the intermolecular distance.[9] It was found that the self-exchange electron-transfer rates increased from $-C(CH_3)_3$ to −H to $-CH_3$, a trend that was not adequately explained by the differences in steric size of the functional groups. This suggested that the electron-withdrawing or -donating nature of the substituents might also influence the measured rates. Additionally, temperature-dependent electrochemical studies indicated that the reorganization energy was insensitive to these functional groups.[9]

In fluid solution, $Ru^{III/II}$ self-exchange rate constants for Ru^{II} polypyridyl compounds are orders of magnitude larger than those of related Ru amine and aquo compounds.[23,24] The π^* orbitals in the bipyridine rings are of the appropriate symmetry and energy to stabilize the $d\pi$ orbitals on the Ru^{II} metal center which leads to the delocalization of the Ru-based $d\pi$ orbitals onto the bipyridine rings.[23,25−28] This π-backbonding effectively places more charge density on the bipyridine ligands and increases the intermolecular coupling H_{DA} relative to the corresponding amine and aquo compounds.[23] Various experimental and computational studies have suggested that 2−25% of electron density of highest occupied molecular orbital in Ru^{II} polypyridyl compounds is located on the π-acidic diimine ligands.[29,30] Therefore, one might expect the electron-withdrawing or -donating groups in the 4 and 4′ positions of the bipyridine ring would tune self-exchange electron-transfer rates by modulating the degree of orbital mixing. Such behavior was reported by Kubiak and co-workers for electron transfer in a series of oxo-centered ruthenium clusters.[31,32] In these studies, it was shown that decreasing the pK_a of 4-substituted pyridine groups coordinated to these clusters increased the self-exchange rate constants over several orders of magnitude. Through NMR studies, they provided clear evidence of enhanced charge density on a pyridine ring as the pK_a decreased. However, when the molecular symmetry prevented significant orbital mixing between the Ru cluster and the π^* orbitals of the pyridine rings, no observable rate enhancement was observed.[31]

In the present study, a series of compounds of the type $[Ru(R_2bpy)_2(P)]^{2+}$, where P is 4,4′-diphosphonic acid-2,2′-bipyridine and R_2bpy is a 4,4′-disubstituted-2,2′-bipyridine with six different R groups: $-OCH_3$, $-C(CH_3)_3$, $-CH_3$, −H, −Br, and $-CF_3$, Scheme 2. The functional groups were chosen to test the effects of both the electron-withdrawing/-donating ability and the steric size on lateral self-exchange electron transfer. Chronoabsorptometry was used to measure the apparent diffusion coefficients, which are proportional to the self-exchange rate constants. Nonadiabatic Marcus theory was used to investigate the interplay of the effects of steric size and the electron-withdrawing or -donating ability of the substituents on $[Ru(R_2bpy)_2(P)]^{3+/2+}$ self-exchange kinetics for compounds anchored to the surface of TiO_2. Variable surface

Scheme 2. Ru^{II} Polypyridyl Compounds Used in this Study

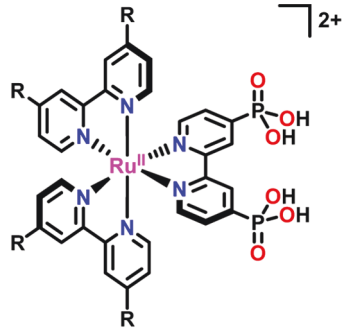

R = $-OCH_3$, $-C(CH_3)_3$, $-CH_3$, -H, -Br, $-CF_3$

DOI: 10.1021/acs.jpcc.8b05281
J. Phys. Chem. C 2018, 122, 19385−19394

coverages were obtained using dilute dyeing solutions. With some assumptions, the variable surface coverage data revealed an exponential dependence of the electron-transfer rate constants with the intermolecular distance. It was concluded that steric size and more specifically the intermolecular distance predominantly determined the rates of self-exchange electron transfer at these TiO_2 interfaces.

EXPERIMENTAL SECTION

Materials. The following solvents and reagents were obtained from the indicated commercial supplier and used without further purification: acetonitrile (CH_3CN, Burdick and Jackson, Spectrophotometric grade); lithium perchlorate ($LiClO_4$, Sigma-Aldrich, 99.99%); perchloric acid ($HClO_4$, Alfa Aesar, 70%), titanium(IV) isopropoxide (Aldrich, ≥97.0%); fluorine-doped tin(IV) oxide (FTO; Hartford Glass Co., Inc., 2.3 mm thick 15 Ω/sq); and oxygen (O_2, Airgas, ≥99.998%). The following compounds were made as previously described or were available from previous studies: $[Ru(MeObpy)_2(P)]Br_2$, $[Ru(dtb)_2(P)]Br_2$, $[Ru(dmb)_2(P)]Br_2$, $[Ru(bpy)_2(P)]Br_2$, $[Ru(Brbpy)_2(P)]Br_2$, and $[Ru(btfmb)_2(P)]Br_2$.[33−39]

Preparation of Thin Films. Titania nanocrystallites were prepared via the hydrolysis of titanium(IV) isopropoxide using the previously reported sol−gel method.[10] Mesoporous thin films were prepared by the doctor blade method on an ethanol-cleaned FTO substrate using Scotch tape (∼50 μm thick) as a spacer to ensure a uniform thickness. The doctor-bladed films were covered and allowed to dry at room temperature for 30 min. Once dry, the films were sintered under an O_2 atmosphere (∼1 atm) for 30 min at 450 °C. These films were stored in a ∼70 °C oven until used. The resulting films were 3−5 μm, as measured using a Bruker Dektak XT profilometer running the Vision 64 software.

The titania thin films were placed into concentrated aqueous dying solutions of the desired $[Ru(R_2bpy)_2(P)]Br_2$ compound in 0.1 M $HClO_4$ to allow for surface functionalization. For studies with variable surface coverages, 25 mL of aqueous solutions of $[Ru(bpy)_2(P)]Br_2$ in 0.1 M $HClO_4$ was made with concentrations ranging from 2 μM to 5 mM for 14 total solutions. Films were submerged for at least 48 h to ensure that uniform, saturation surface coverages were achieved. Prior to use, the films were soaked in neat CH_3CN solutions for at least 1 h to remove any weakly adsorbed molecules from the surface to minimize dye desorption during the course of the experiments.

Spectroscopy. All steady-state UV−visible spectra were recorded on an AvaSpec UL2048 UV−visible spectrometer and an AvaLight deuterium/halogen light source (Avantes) at room temperature. All measurements were obtained using a 1 cm^2 cuvette with the functionalized titania films placed along the diagonal at a 45° angle to the incident probe light.

Chronoabsorptometry. Chronoabsorptometry (CA) was performed using a WaveNow potentiostat (Pine Research Instrumentation, Inc.) coupled to an AvaSpec UL2048 UV−visible spectrometer and an AvaLight deuterium/halogen light source (Avantes) all controlled by the AfterMath software (Pine Research Instrumentation, Inc.). A standard three-electrode arrangement was used with the functionalized titania films as the working electrode, a Pt mesh counter electrode, a Ag/AgCl pseudoreference electrode. The nonaqueous Ag/AgCl pseudoreference electrode (Pine Research Instrumentation, Inc.) was filled with a 0.1 M $LiClO_4$ solution in CH_3CN, and the applied potential was referenced to the $E_{1/2}(Ru^{III/II})$ of the $[Ru(R_2bpy)_2(P)]^{2+}$ on the surface. To measure D_{CA}, a potential of $E_{1/2}(Ru^{III/II})$ + 500 mV was applied, and full UV−visible spectra were taken at fixed time intervals. All chronoabsorptometry studies were performed using CH_3CN solutions containing 0.1 M $LiClO_4$.

To measure the $E_{1/2}(Ru^{III/II})$, cyclic voltammetry was used with the same three-electrode arrangement as described above using a 0.1 M $LiClO_4$ solution in CH_3CN. For these measurements, the pseudoreference electrode was externally calibrated versus the ferrocenium/ferrocene ($Fc^{+/0}$) reduction potential in a CH_3CN solution containing 0.2 M $LiClO_4$, which is 0.31 V vs the standard calomel electrode (SCE).[40] SCE is 0.241 V vs the normal hydrogen electrode (NHE).[40] All potentials reported are vs NHE unless otherwise stated.

Data Analysis. Data fitting was performed in OriginPro 2016, with least-squares error minimization achieved using the Levenberg−Marquardt method. The errors reported for fitting parameters are the standard errors. The errors reported for the $[Ru(R_2bpy)_2(P)]|TiO_2$ data were quantified as a standard deviation of 2−3 trials. The errors reported for the variable surface coverage data were obtained through the propagation of error for all of the values utilized.

RESULTS

A series of 6 Ru^{II} polypyridyl compounds of the type $[Ru(R_2bpy)_2(P)]Br_2$, where R_2bpy is a 4,4′-substituted-2,2′-bipyridine and P is a 2,2′-bipyrdyl-4,4′-diphosphonic acid, was synthesized using standard methods, Scheme 2.[37] The R groups used were $-OCH_3$, $-C(CH_3)_3$, $-CH_3$, −H, −Br, and $-CF_3$ (MeObpy, dtb, dmb, bpy, Brbpy, and btfmb, respectively). These functional groups were chosen to allow for wide range of variability in electron-withdrawing or -donating strength as well as steric size.

The TiO_2 thin films were functionalized with the desired $[Ru(R_2bpy)_2(P)]Br_2$ from concentrated dyeing solution in aqueous 0.1 M $HClO_4$ solutions. Thin films were left submerged for a minimum of 48 h to ensure the saturation surface coverage, Γ_0, was reached. Upon functionalization, the films displayed the characteristic metal-to-ligand charge transfer (MLCT) bands of $[Ru(R_2bpy)_2(P)]^{2+}$ compounds, Figure 1. Assuming that the absorbance maximum, λ_{MLCT}, and

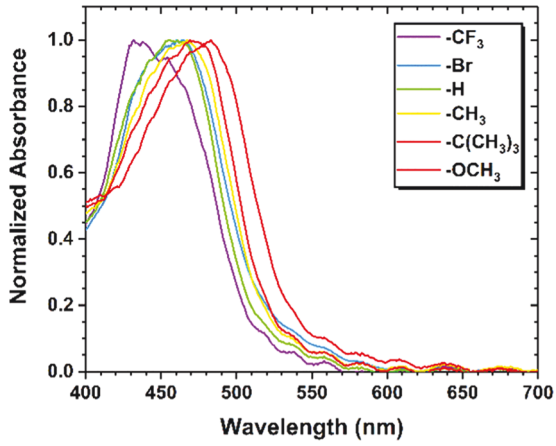

Figure 1. Normalized UV−visible absorbance spectra for each $[Ru(R_2bpy)_2(P)]|TiO_2$ film submerged in CH_3CN solutions containing 0.1 M $LiClO_4$ with an unsensitized thin film as a reference.

DOI: 10.1021/acs.jpcc.8b05281
J. Phys. Chem. C 2018, 122, 19385−19394

Table 1. Relevant Electrochemical and Photophysical Properties of the $[Ru(R_2bpy)_2(P)](Br)_2$ Compounds

	λ_{MLCT} (nm)[a] (ε 10^4 M^{-1} cm^{-1})	$E_{1/2}(Ru^{III/II})$[e] (V vs NHE)	D_{CA} (10^{-9} cm^2/s)	Γ_0 (10^{-8} mol × cm^{-2} × μm^{-1})	δ (nm)	k_R (10^5 s^{-1})
$-OCH_3$	477 (1.18)[b]	1.24	7.9 ± 0.3	2.24 ± 0.03	1.64 ± 0.01	17.6 ± 0.7
$-C(CH_3)_3$	460 (1.40)[c]	1.37[c]	0.4 ± 0.2	1.6 ± 0.2	1.83 ± 0.06	0.7 ± 0.4
$-CH_3$	461 (1.28)[b]	1.38	4 ± 1	2.0 ± 0.4	1.7 ± 0.1	8 ± 2
$-H$	458 (1.20)[b]	1.44	5.1 ± 0.2	2.41 ± 0.05	1.60 ± 0.01	11.9 ± 0.5
$-Br$	465 (1.34)[b]	1.58	7 ± 1	3.1 ± 0.2	1.48 ± 0.04	19 ± 2
$-CF_3$	460 (1.66)[d]	1.74	0.028 ± 0.004	1.18 ± 0.02	2.04 ± 0.01	0.040 ± 0.06

[a]Reported in H_2O due to low solubility in CH_3CN. [b]Value taken from ref 37. [c]Value taken from ref 39. [d]Value taken from ref 38. [e]Measured in 0.1 M $LiClO_4$ solutions in CH_3CN. Error in the reported values is ±10 mV.

the molar absorptivity coefficient, ε, remain unchanged on the surface relative to solution, Γ_0 was calculated using eq 3, where A_{MLCT} is the absorbance at λ_{MLCT}. To account for the pathlength of the film, the incidence angle of the probe beam (45°) and the refractive index (1.59) measured for similar mesoporous, nanocrystalline TiO_2 thin films were used.[41] Through the Snell–Descartes law, the angle of refraction through the film was determined to be 36.7°, and $d/\cos(36.7°)$ was added to eq 3 to adjust the measured surface coverage for the thickness of the film. Note that Γ_0 calculated in this way has units of mol × cm^{-2} × μm^{-1} and corrects for any film-to-film thickness variations. The measured Γ_0 as well as the relevant spectroscopic properties for these compounds are listed in Table 1.

$$A = 1000 \times \Gamma_0 \times \varepsilon \times (d/\cos(36.7°)) \quad (3)$$

Cyclic voltammetry was used to determine the half wave potentials, $E_{1/2}(Ru^{III/II})$, of the sensitized thin film in 0.1 M $LiClO_4$ CH_3CN solutions. The cyclic voltammograms displayed quasi-reversible waves with peak-to-peak splitting between 100 and 300 mV.[10] The measured values ranged from 1.24 to 1.74 V vs NHE and were consistent with the one-electron oxidation of the compounds, Table 1. The measured half wave potentials increased with the electron-withdrawing ability of the functional groups.

To investigate the substituent effects on self-exchange electron-transfer rates between surface-immobilized compounds, chronoabsorptometry (CA) was performed utilizing 0.1 M $LiClO_4/CH_3CN$ electrolyte solutions. In these experiments, a potential step 500 mV more positive than the $E_{1/2}(Ru^{III/II})$ was applied to oxidize the $[Ru(R_2bpy)_2(P)]|TiO_2$, and the spectral changes were monitored as a function of time. Figure 2 shows representative data for $[Ru(dtb)_2(P)]|TiO_2$, and spectra for all other $[Ru(R_2bpy)_2(P)]|TiO_2$ can be found in the Supporting Information. Upon oxidation, all of the compounds exhibited a loss of the characteristic Ru^{II} MLCT transition and a growth of a weak, broad absorbance feature at wavelengths above 600 nm. Both spectral changes were indicative of the one-electron oxidation of the compound from Ru^{II} to Ru^{III}.

Single-wavelength kinetics were monitored at the λ_{MLCT} and were plotted as the normalized absorbance change, ΔA, versus the square root of time, t, Figure 3, for all six compounds. These data were fit to the Anson equation, eq 4, where D_{CA} is the apparent diffusion. The calculated D_{CA} values are given in Table 1. The Anson equation was previously derived using semi-infinite diffusion boundary conditions for molecules diffusing to the electrode surface.[9,11,12] Here, Ru^{II} polypyridyl compounds were anchored to the TiO_2 film of a finite thickness. Therefore, the data deviate from the predicted linear

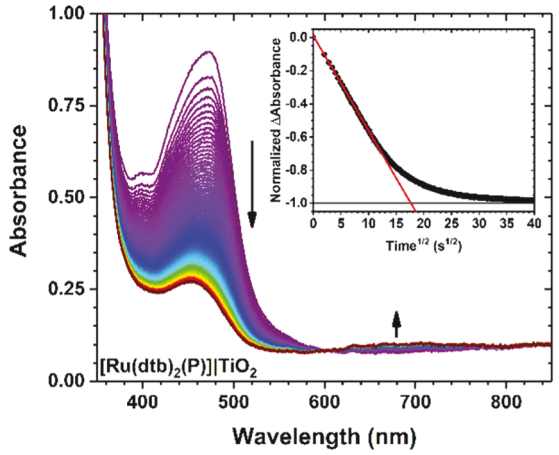

Figure 2. UV–visible absorption spectra measured after the application a potential sufficient to oxidize $[Ru(dtb)_2(P)]|TiO_2$. A bleach of the characteristic MLCT transition was observed at 470 nm as the film was oxidized from Ru^{II} to Ru^{III}. A new absorption feature associated with the Ru^{III} species was observed to grow in centered at 675 nm. The inset shows the normalized absorbance change plotted against the square root of time. The data were fit to the Anson equation through the first 60% of the total absorbance change (red line).

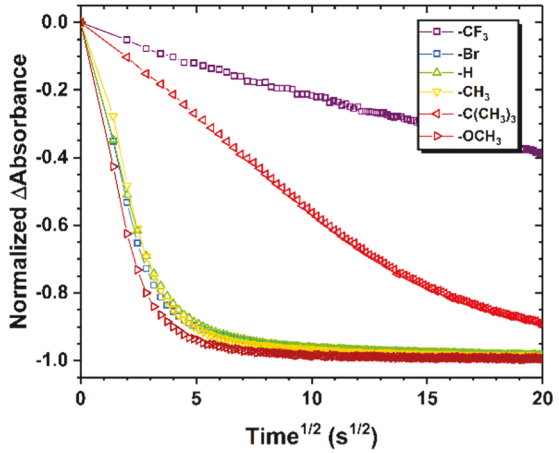

Figure 3. Normalized change in absorbance after the application of sufficiently positive potential to oxidize the $[Ru(R_2bpy)_2(P)]|TiO_2$, plotted as a function of the square root of time for all compounds used in this study.

relationship described by the Anson equation, Figure 2 inset and Figure 3. It has been shown by several groups that a linear relationship is maintained for the first 60% of the total absorbance change in CA experiments.[9,11,12] Thus, only 60% of

DOI: 10.1021/acs.jpcc.8b05281
J. Phys. Chem. C 2018, 122, 19385–19394

the total change was fit during the analysis, inset Figure 2 for $[Ru(dtb)_2(P)]|TiO_2$ and Supporting Information for the others. The smallest D_{CA} measured was 2.8×10^{-11} cm^2/s for $[Ru(CF_3bpy)_2(P)]|TiO_2$ followed by $[Ru(dtb)_2(P)]|TiO_2$, which was an order of magnitude larger with a value of 3.6×10^{-10} cm^2/s. The other four compounds measured all had diffusion coefficients that were on the same order of magnitude with values between 3.8×10^{-9} and 7.9×10^{-9} cm^2/s. These values agreed with those published for similar Ru^{II} polypyridyl compounds anchored to TiO_2 with phosphonic acid and carboxylic acid binding groups.[6,9,13,17,42] Throughout the course of the experiments, no desorption of the surface-bound compounds was observed.

$$\Delta A = \frac{2D^{1/2}t^{1/2}}{d\pi^{1/2}} \tag{4}$$

As a control to test the effects of intermolecular distance, the apparent diffusion coefficients were measured for films at subsaturation surface coverages. Subsaturation surface coverages were achieved by functionalizing the films from aqueous 0.1 M $HClO_4$ solutions of different concentrations of $[Ru(bpy)_2(P)]Br_2$ that ranged from 2 μM to 5 mM and resulted in surface coverages between 4.4×10^{-9} and 6.2×10^{-8} mol $\times$ $cm^{-2} \times \mu m^{-1}$. The diffusion coefficient for electron transfer was measured for each of these films, Figure 4. The

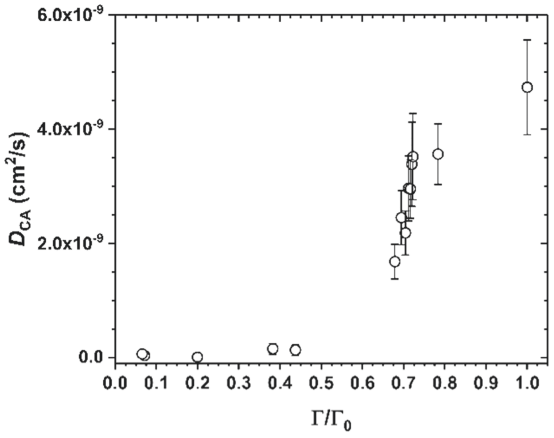

Figure 4. Variation of the measured apparent diffusion coefficients (D_{CA}) for $[Ru(bpy)_2(P)]|TiO_2$ with the fractional surface coverage (Γ/Γ_0), where Γ_0 was the maximum surface coverage attained in the most concentrated dyeing solution (5 mM). The D_{CA} was measured in CH_3CN solutions with 0.1 M $LiClO_4$ electrolyte. Error bars for D_{CA} included for all data.

onset for self-exchange electron transfer, i.e., the percolation threshold, was between 50 and 60% of the saturation surface coverage and was in agreement with what has been reported previously for Ru^{II} polypyridyl compounds.[6,13] The observation of a percolation threshold also indicated that physical diffusion of the molecules was not contributing significantly to the measured diffusion coefficients.[43,44]

Conversion of the measured diffusion coefficients to a first-order self-exchange "hopping" rate constant, k_R, required knowledge of the intermolecular distance, δ, between the molecules on the interface. The value of δ is unknown, and estimates based on critical assumptions were made. It was assumed that the molecules were evenly distributed within the pore volume of the TiO_2 from the measured Γ_0 using eq 5 where $\Gamma \times 10^4$ is the surface coverage converted to concentration with units of mol/cm^3, N is Avogadro's number, and p is the porosity, which was assumed to be 60%.[45] This "concentration" was converted to an intermolecular distance with the assumption that the molecules were in a cubic lattice arrangement using $\delta = (c_0)^{-1/3}$, as has been done previously.[9,16] Note that the δ calculated with these assumptions represents an upper limit as the compounds were assumed to be evenly distributed, and any aggregation was not taken into account. With the computed δ, the k_R was calculated for each compound using the Dahms−Ruff equation, eq 6.[9,13,43]

$$c_0 = \frac{(\Gamma_0 \times 10^4) \times N}{p} \tag{5}$$

$$D_{CA} = \frac{k_R\delta^2}{6} \tag{6}$$

DISCUSSION

A detailed understanding of the synthetic handles available to tune lateral self-exchange electron-transfer rates at semiconductor interfaces is important for the optimization of many solar energy conversion schemes.[1−8] Previous work to determine if small structural changes in a homologous series of Ru^{II} polypyridyl compounds of the type $[Ru(R_2bpy)_2(dcb)]^{2+}$, where R_2bpy was a 4,4′-substituted-2,2′-bipyridine and dcb was 2,2′-bipyridyl-4,4′-dicarboxylic acid, revealed that substituents in the 4 and 4′ positions of the bipyridine rings did influence the self-exchange rate though it was unclear if the variation in the measured apparent diffusion coefficients, D_{CA}, was due to the steric size, the relative electron-withdrawing or -donating ability, or both for the chosen functional groups.[9] Here, an expanded series of Ru^{II} polypyridyl compounds of the type $[Ru(R_2bpy)_2(P)]^{2+}$, where P is 2,2′-bipyrdyl-4,4′-diphosphonic acid, was reported with a wide variety of functional groups of varying electron-withdrawing or -donating strengths and steric sizes to elucidate the degree of influence each had on lateral self-exchange. Chronoabsorptometry was used to quantify the D_{CA}, and the measured values were analyzed within the framework of nonadiabatic Marcus theory. The data indicated that the substituent steric size was the main factor that influenced lateral self-exchange through variations in surface coverage and thus intermolecular distance.

Quantification of Reduction Potentials and Apparent Diffusion Coefficients. The $Ru^{III/II}$ formal reduction potentials, $E_{1/2}(Ru^{III/II})$, were measured for each compound anchored to the TiO_2 interface using cyclic voltammetry in 0.1 M $LiClO_4$ in CH_3CN. The peak-to-peak separation between the cathodic and anodic waves in the cyclic voltammogram fell between 100 and 300 mV, which was consistent of a quasi-reversible electrochemical process.[10] The measured $E_{1/2}(Ru^{III/II})$ reflects the energy of the $d\pi$ orbitals. As such, comparing the $E_{1/2}(Ru^{III/II})$ between the compounds anchored to the surface reports directly on the degree of stabilization imparted on the Ru $d\pi$ orbitals from π-backbonding with the bipyridine π^* orbitals. $[Ru(MeObpy)_2(P)]|TiO_2$ possessed the least positive $E_{1/2}(Ru^{III/II})$, 1.24 V vs NHE, whereas $[Ru(btfmb)_2(P)]|TiO_2$ was the most positive, 1.74 V vs NHE. These observations agreed with the notion that the electron-withdrawing groups stabilize the π^* orbitals of the bipyridine rings and increased the π-acidity of the orbitals.[25−28] In fact,

DOI: 10.1021/acs.jpcc.8b05281
J. Phys. Chem. C 2018, 122, 19385−19394

the summative Hammett parameter, σ_T, of each compound given by eq 7, was found to be strongly correlated with the measured $E_{1/2}(Ru^{III/II})$, Figure 5. In eq 7, the sum of the

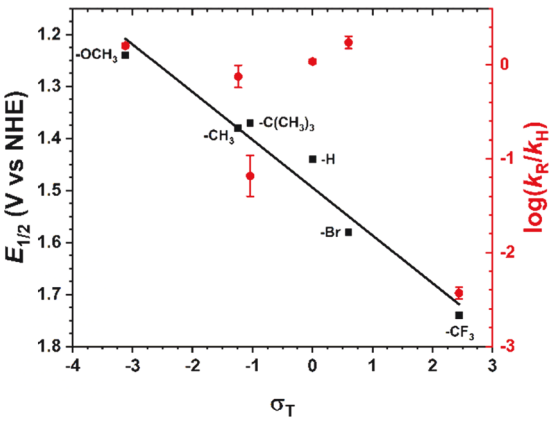

Figure 5. Dependence of the measured $E_{1/2}(Ru^{III/II})$ (black, ■) and of $\log(k_H/k_R)$ (red, ●) on the summative Hammett parameter, σ_T, for all $[Ru(R_2bpy)_2(P)]|TiO_2$. The measured $E_{1/2}(Ru^{III/II})$ displayed a strong correlation with σ_T with a slope of 0.09 V. No such correlation was observed with $\log(k_H/k_R)$. Error bars are given for the $\log(k_H/k_R)$ data.

Hammett parameters for para-substitution, σ_p^+, is summed for all of the substituents on the bipyridine rings. The σ_p^+ values were used to reflect the substituents ability to stabilize the increasing positive charge in the transition state during Ru^{II} oxidation through resonance. Note that the σ_p^+ values have been previously shown to correlate well with $E_{1/2}(Ru^{III/II})$ for substituted Ru^{II} polypyridyl compounds.[27,28] The slope of the line in Figure 5 provided by linear regression was 0.09 V and matched values reported for similar analysis with Ru^{II} tris(bipyridyl)-type compounds.[27] Both σ_p^+ and σ_T for each compound are listed in Table 2. Note that the $-PO(OH)_2$

Table 2. Selected Hammett and Charton Parameters[46,47]

	Hammett parameter[a] (σ_p^+)	summative Hammett parameter[b] (σ_T)	Charton parameter (ν)
$-OCH_3$	−0.78	−3.12	0.36
$-C(CH_3)_3$	−0.26	−1.04	1.24
$-CH_3$	−0.31	−1.24	0.52
−H	0	0	0
−Br	0.15	0.60	0.65
$-CF_3$	0.61	2.44	0.91

[a]Value given for a single substituent. [b]Value given for $[Ru(R_2bpy)_2(P)]^{2+}$ omitting the contribution from the $-PO(OH)_2$ function groups.

substituents were not included in σ_T as no values of σ_p^+ were found in the literature; however, the slope in Figure 5 would remain unchanged with or without their inclusion since the σ_T for each compound has the same contribution from $-PO(OH)_2$.

$$\sigma_T = \sum_i \sigma_p^+ \quad (7)$$

Chronoabsorptometry (CA) allowed for the measurement of the apparent diffusion coefficients, D_{CA}, for each compound at the TiO_2 interface. The D_{CA} values were used as an analog to the second-order self-exchange electron-transfer rate constants, k_R', for compounds anchored to the interface as they are directly proportional to one another, eq 6.[11−13,16] However, direct measurement of k_R' was difficult because of the nebulousness of concentration at these interfaces. The measured D_{CA} values were between 10^{-11} and 10^{-9} cm^2/s. These values were consistent with other reported values for Ru^{II} polypyridyl compounds measured by CA.[6,9,17,48] Previous studies with $[Ru(bpy)_2(P)]|TiO_2$ reported D_{CA} values to be between 1.1×10^{-9} and 1.3×10^{-9} cm^2/s.[6,17] These values were about a factor 2 smaller than the value measured here. In those reports, the surface coverages were smaller than those reported here for the same compound, which would result in a smaller D_{CA} value (vide infra). DiMarco and co-workers previously concluded that $[Ru(CF_3bpy)_2(dcb)]|TiO_2$ displayed no or extremely slow lateral self-exchange electron transfer under the conditions of their study.[2] This was consistent with the small D_{CA} value measured for $[Ru(CF_3bpy)_2(P)]|TiO_2$ reported here.

It is often more convenient to convert the measured D_{CA} values to a first-order hopping rate constant, k_R, to compare the measured rates with other techniques; however, one must make numerous assumptions about the molecular arrangement at the interface. Here, it was assumed that the compounds were arranged in a cubic lattice pattern within the pore volume of the film. The intermolecular distances calculated in this way necessarily represented an upper limit to the intermolecular spacing as it is often asserted that the molecules form a monolayer and are not freely diffusing in the pores.[13] The k_R values were calculated to be between 10^3 and 10^6 s^{-1}. In operational dye-sensitized solar cells, photoinitiated excited-state electron injection from the surface-bound molecule leaves behind an oxidized chromophore that can undergo self-exchange electron transfer.[13,49] Lateral self-exchange hopping rate constants measured under these conditions were found to be on the order of 10^6 s^{-1} for both $[Ru(dmb)_2(dcb)]|TiO_2$ and $[Ru(dtb)_2(dcb)]|TiO_2$ measured by nanosecond transient absorption spectroscopy.[8,50] These values are 1−2 orders of magnitude larger than what was calculated from the D_{CA}. In these studies, interparticle electron transfer must occur to oxidize the entire thin film. This differs from previous anisotropy studies where hole hopping occurs in kinetic competition with charge recombination.[8,50,51] Though speculative, it may be that electron transfer between molecules on different TiO_2 particles is slower than between those on the same nanoparticle, which would be reflected in the rate constants reported.

Substituent Effects on Self-Exchange Electron Transfer at the Interface. Marcus theory has been successfully and extensively applied to describe and predict electron transfer between donor and acceptor compounds, including self-exchange electron transfer between Ru^{II} polypyridyl compounds in fluid solution and anchored to semiconductor interfaces.[9,18,24] For self-exchange electron transfer where $\Delta G^\circ = 0$ on TiO_2, λ has been reported to be independent of the 4,4′-substituents.[9] Instead changes in k_R were attributed to the mixing of the donor and acceptor wavefunctions, H_{DA}, through increasing the intermolecular distance (steric size).

As shown above, the measured $E_{1/2}(Ru^{III/II})$ values displayed a strong linear correlation with σ_T values that was indicative of the better energetic overlap between the Ru-based $d\pi$ and bpy-based π^* orbitals with increasing electron-withdrawing strength. This enhanced overlap would lead to more orbital mixing as reported by Kubiak et al. for oxo-centered ruthenium

DOI: 10.1021/acs.jpcc.8b05281
J. Phys. Chem. C 2018, 122, 19385−19394

clusters.[31,32] If the enhanced delocalization affected self-exchange electron transfer at the interface, one would also expect a correlation of the first-order hopping rate constants with σ_T as described by eq 8, where ρ is the sensitivity factor of lateral self-exchange electron transfer to the electron-withdrawing or -donating ability of the functional groups, R is the gas constant, $\Delta\Delta G^{\ddagger}$ is the differences in the free energy of activation between $[Ru(bpy)_2(P)]|TiO_2$ ($\Delta G_H^{\ddagger}$) and $[Ru(R_2bpy)_2(P)]|TiO_2$ ($\Delta G_R^{\ddagger}$), and k_H and k_R are the first-order hopping rate constants for $[Ru(bpy)_2(P)]|TiO_2$ and $[Ru(R_2bpy)_2(P)]|TiO_2$, respectively.[47,52] However, no correlation was observed between $\ln(k_R/k_H)$ and σ_T, Figure 5. This implies that there was no significant change in the intermolecular coupling as the energetic separation between the $d\pi$ orbitals and the π^* orbitals became smaller. In the nonadiabatic limit of Marcus theory, the $\Delta G_R^{\ddagger}$ is described by eq 9.[24] Since λ has been previously reported to be invariant to the identity of the alkyl functional groups, it would be expected that $\Delta\Delta G^{\ddagger}$ is equal to 0 in the absence of significant orbital delocalization, and no correlation of $\ln(k_R/k_H)$ and σ_T would be observed.

$$\ln\frac{k_R}{k_H} = \frac{\Delta\Delta G^{\ddagger}}{RT} = \rho\sigma_T \tag{8}$$

$$\Delta G_R^{\ddagger} = \frac{\lambda}{4} \tag{9}$$

The steric bulk of the 4 and 4′ substituents have been shown to decrease the saturation surface coverages, Γ_0, for Ru^{II} polypyridyl compounds.[9,15] Therefore, it was expected that the substituents used here would also influence the surface coverage. One measure of the steric size of substituents is known as the Charton value, ν, and is derived from the difference in the van der Waals radii of a given substituent and a proton.[53,54] Figure 6 shows the relationship between Γ_0 and

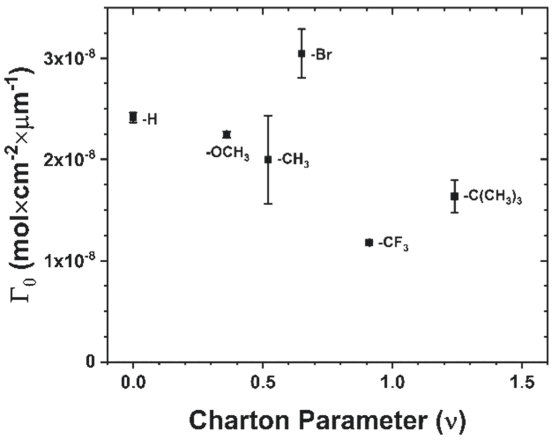

Figure 6. Dependence of the saturation surface coverage, Γ_0, with the steric size of the substituent in the 4 and 4′ positions of $[Ru(R_2bpy)_2(P)]|TiO_2$ as given by the Charton value. Error bars are included for the measured Γ_0.

ν. Several observations are clear from these data. First, as the steric size of the aliphatic groups increased, the measured Γ_0 decreased, as was previously reported.[9] Second, $[Ru(btfmb)_2(P)]|TiO_2$ yielded a smaller surface coverage than expected. Fluorinated alkyl groups have been reported to be larger than their nonfluorinated congener, behavior attributed to a large electronic repulsion of the electron clouds around the strongly electronegative F atoms.[55] It has also been noted that typical measures of steric size often underestimate the size of these fluorinated groups.[55] Thus, the small Γ_0 value for $[Ru(btfmb)_2(P)]|TiO_2$ was not unexpected. Finally, the −Br substituents resulted in the largest surface coverages despite their atomic size relative to an H atom. Typically, Langmuir-type binding is used to describe surface functionalization of TiO_2 thin films, which assumes that intermolecular interactions do not influence surface binding.[13] In the case of the −Br, it may be that halogen bonding interactions between a halogen and a $-PO(OH)_2$ on a neighboring compound may act as directing groups, as the molecules approach the surface leading to more efficient packing and higher surface coverages.[56,57]

As stated in the introduction, the intermolecular electronic coupling is expected to have an exponential dependence on intermolecular distance, eq 2. In the absence of measured H_{DA} values in these self-exchange reactions, the calculated first-order hopping rate constants were used to compare the differences in electronic coupling, eq 10, where $\Delta\delta$ is the difference between the calculated δ and the smallest δ for a given dataset. These data are plotted in Figure 7 from which it

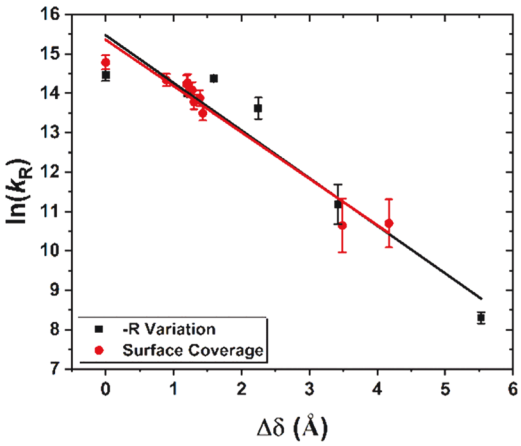

Figure 7. $Ru^{III/II}$ lateral self-exchange electron-transfer rate constant versus the difference in intermolecular distance, $\Delta\delta$. The distance was varied by either (A, black ■) changing the steric size of the -R group at the 4 and 4′ positions (β = 1.2 ± 0.2 Å^{-1}) or (B, red ●) functionalizing the TiO_2 with $[Ru(bpy)_2(P)]^{2+}$ from dilute dying solutions (β = 1.18 ± 0.09 Å^{-1}). Error bars are given for the $\ln(k_R)$.

is clear that the measured lateral self-exchange rate constants correlate well with the intermolecular distance determined from the measured surface coverages. From the slope, β was determined to be 1.2 ± 0.2 Å^{-1} for $Ru^{III/II}$ self-exchange across the semiconductor surface. Note that this β value represents a lower limit based on the assumptions used to calculate δ.

$$k_R = e^{-\beta\Delta\delta_R} \tag{10}$$

The apparent diffusion coefficient was measured for $[Ru(bpy)_2(P)]|TiO_2$ at variable surface coverages and the distance dependence examined as above. The β was found to be 1.18 ± 0.09 Å^{-1}, which was reasonably close to that obtained from data where the functional groups were varied. The similarity of the β values coupled with the expected exponential distance dependence strongly suggests that the variation in the measured k_R values with Ru compounds that possess different functional groups results from an underlying distance effect.

DOI: 10.1021/acs.jpcc.8b05281
J. Phys. Chem. C 2018, 122, 19385−19394

To our knowledge, these are the first estimated β values for lateral self-exchange electron transfer between molecules anchored to a TiO_2 interface. Typical attenuation factors reported for bimolecular electron transfer between compounds in frozen and fluid solutions range from 0.8 to 1.5 $Å^{-1}$.[18,20,21,58−61] β values of 0.95 and 1.2 $Å^{-1}$ have been reported for inter- and intramolecular electron transfer in acetonitrile.[60,62] Hence, although it is unclear how the TiO_2 interface and the structure of the double-layer influence the intermolecular coupling, the β values estimated here are in the same range as those reported for organic solutions.

CONCLUSIONS

A homologous series of six compounds of the type $[Ru(R_2bpy)_2(P)]|TiO_2$, where P is 2,2′-bipyrdyl-4,4′-diphosphonic acid and R_2bpy is a 4,4′-substituted-2,2′-bipyridine is reported, and their lateral self-exchange electron-transfer kinetics across the metal oxide surface were quantified. The measured apparent diffusion coefficients ranged from 10^{-11} to 10^{-9} cm^2/s. The 4,4′-functional groups ($-OCH_3$, $-C(CH_3)_3$, $-CH_3$, −H, −Br, and $-CF_3$) were chosen with the expectation that these would provide information on how the electron density of the bipyridine ligands influences hole hopping. However, it was experimentally found that the steric size of the functional group was the key factor. With some assumptions, a measured attenuation factor $\beta = 1.2 \pm 0.2$ $Å^{-1}$ was determined that is in the range expected for electron transfer in fluid acetonitrile. The results herein further indicate that sterics are a reliable synthetic tool that can be used to tune the self-exchange electron-transfer rates across semiconductor interfaces.

ASSOCIATED CONTENT

Supporting Information

The Supporting Information is available free of charge on the ACS Publications website at DOI: 10.1021/acs.jpcc.8b05281.

UV−visible spectra obtained during the chronoabsorptometry experiments with the fitted data for $[Ru(MeObpy)_2(P)]|TiO_2$, $[Ru(dmb)_2(P)]|TiO_2$, $[Ru(bpy)_2(P)]|TiO_2$, $[Ru(Brbpy)_2(P)]|TiO_2$, and $[Ru(btfmb)_2(P)]|TiO_2$ (PDF)

AUTHOR INFORMATION

Corresponding Author

*E-mail: gjmeyer@email.unc.edu. Phone: 1-919-962-6320.

ORCID

Tyler C. Motley: 0000-0002-7749-9183

Matthew D. Brady: 0000-0002-3917-1072

Gerald J. Meyer: 0000-0002-4227-6393

Notes

The authors declare no competing financial interest.

ACKNOWLEDGMENTS

This research is supported by the National Science Foundation (NSF) under Award CHE-1465060. T.C.M. would like to acknowledge the NSF Graduate Research Fellowship for support (Grant No. DGE-1144081).

REFERENCES

(1) Moia, D.; Szumska, A.; Vaissier, V.; Planells, M.; Robertson, N.; O'Regan, B. C.; Nelson, J.; Barnes, P. R. F. Interdye Hole Transport Accelerates Recombination in Dye Sensitized Mesoporous Films. *J. Am. Chem. Soc.* **2016**, *138*, 13197−13206.

(2) Sampaio, R. N.; DiMarco, B. N.; Meyer, G. J. Activation Energies for Electron Transfer from TiO_2 to Oxidized Dyes: A Surface Coverage Dependence Correlated with Lateral Hole Hopping. *ACS Energy Lett.* **2017**, *2*, 2402−2407.

(3) Sampaio, R. N.; Müller, A. V.; Polo, A. S.; Meyer, G. J. Correlation Between Charge Recombination and Lateral Hole-Hopping Kinetics in a Series of cis-$Ru(phen')(dcb)(NCS)_2$ Dye-Sensitized Solar Cells. *ACS Appl. Mater. Interfaces* **2017**, *9*, 33446−33454.

(4) Moia, D.; Leijtens, T.; Noel, N.; Snaith, H. J.; Nelson, J.; Barnes, P. R. F. Dye Monolayers Used as the Hole Transporting Medium in Dye-Sensitized Solar Cells. *Adv. Mater.* **2015**, *27*, 5889−5894.

(5) Moia, D.; Cappel, U. B.; Leijtens, T.; Li, X.; Telford, A. M.; Snaith, H. J.; O'Regan, B. C.; Nelson, J.; Barnes, P. R. F. The Role of Hole Transport between Dyes in Solid-State Dye-Sensitized Solar Cells. *J. Phys. Chem. C* **2015**, *119*, 18975−18985.

(6) Swierk, J. R.; McCool, N. S.; Saunders, T. P.; Barber, G. D.; Mallouk, T. E. Effects of Electron Trapping and Protonation on the Efficiency of Water-Splitting Dye-Sensitized Solar Cells. *J. Am. Chem. Soc.* **2014**, *136*, 10974−10982.

(7) Hu, K.; Sampaio, R. N.; Marquard, S. L.; Brennaman, M. K.; Tamaki, Y.; Meyer, T. J.; Meyer, G. J. A High-Valent Metal-Oxo Species Produced by Photoinduced One-Electron, Two-Proton Transfer Reactivity. *Inorg. Chem.* **2018**, *57*, 486−494.

(8) Chen, H.-Y.; Ardo, S. Direct Observation of Sequential Oxidations of a Titania-Bound Molecular Proxy Catalyst Generated through Illumination of Molecular Sensitizers. *Nat. Chem.* **2017**, *10*, 17−23.

(9) DiMarco, B. N.; Motley, T. C.; Balok, R. S.; Li, G.; Siegler, M. A.; O'Donnell, R. M.; Hu, K.; Meyer, G. J. A Distance Dependence to Lateral Self-Exchange across Nanocrystalline TiO_2. A Comparative Study of Three Homologous $Ru^{III/II}$ Polypyridyl Compounds. *J. Phys. Chem. C* **2016**, *120*, 14226−14235.

(10) Heimer, T. A.; D'Arcangelis, S. T.; Farzad, F.; Stipkala, J. M.; Meyer, G. J. An Acetylacetonate-Based Semiconductor−Sensitizer Linkage. *Inorg. Chem.* **1996**, *35*, 5319−5324.

(11) Bonhôte, P.; Gogniat, E.; Tingry, S.; Barbé, C.; Vlachopoulos, N.; Lenzmann, F.; Comte, P.; Grätzel, M. Efficient Lateral Electron Transport inside a Monolayer of Aromatic Amines Anchored on Nanocrystalline Metal Oxide Films. *J. Phys. Chem. B* **1998**, *102*, 1498−1507.

(12) Trammell, S. A.; Meyer, T. J. Diffusional Mediation of Surface Electron Transfer on TiO_2. *J. Phys. Chem. B* **1999**, *103*, 104−107.

(13) Hu, K.; Meyer, G. J. Lateral Intermolecular Self-Exchange Reactions for Hole and Energy Transport on Mesoporous Metal Oxide Thin Films. *Langmuir* **2015**, *31*, 11164−11178.

(14) Wang, Q.; Zakeeruddin, S. M.; Cremer, J.; Bäuerle, P.; Humphry-Baker, R.; Grätzel, M. Cross Surface Ambipolar Charge Percolation in Molecular Triads on Mesoscopic Oxide Films. *J. Am. Chem. Soc.* **2005**, *127*, 5706−5713.

(15) Wang, Q.; Zakeeruddin, S. M.; Nazeeruddin, M. K.; Humphry-Baker, R.; Grätzel, M. Molecular Wiring of Nanocrystals: NCS-Enhanced Cross-Surface Charge Transfer in Self-Assembled Ru-Complex Monolayer on Mesoscopic Oxide Films. *J. Am. Chem. Soc.* **2006**, *128*, 4446−4452.

(16) Moia, D.; Vaissier, V.; Lopez-Duarte, I.; Torres, T. S.; Nazeeruddin, M. K.; O'Regan, B. C.; Nelson, J.; Barnes, P. R. F. The Reorganization Energy of Intermolecular Hole Hopping between Dyes Anchored to Surfaces. *Chem. Sci.* **2014**, *5*, 281−290.

(17) Hanson, K.; Brennaman, M. K.; Ito, A.; Luo, H.; Song, W.; Parker, K. A.; Ghosh, R.; Norris, M. R.; Glasson, C. R. K.; Concepcion, J. J.; Lopez, R.; Meyer, T. J. Structure−Property Relationships in Phosphonate-Derivatized, Ru^{II} Polypyridyl Dyes on Metal Oxide Surfaces in an Aqueous Environment. *J. Phys. Chem. C* **2012**, *116*, 14837−14847.

(18) Marcus, R. A.; Sutin, N. Electron Transfers in Chemistry and Biology. *Biochim. Biophys. Acta, Rev. Bioenerg.* **1985**, *811*, 265−322.

(19) Winkler, J. R.; Gray, H. B. Long-Range Electron Tunneling. *J. Am. Chem. Soc.* **2014**, *136*, 2930−2939.
(20) Wenger, O. S.; Leigh, B. S.; Villahermosa, R. M.; Gray, H. B.; Winkler, J. R. Electron Tunneling Through Organic Molecules in Frozen Glasses. *Science* **2005**, *307*, 99−102.
(21) Edwards, P. P.; Gray, H. B.; Lodge, M. T. J.; Williams, R. J. P. Electron Transfer and Electronic Conduction through an Intervening Medium. *Angew. Chem., Int. Ed.* **2008**, *47*, 6758−6765.
(22) Closs, G. L.; Miller, J. R. Intramolecular Long-Distance Electron Transfer in Organic Molecules. *Science* **1988**, *240*, 440−447.
(23) Brown, G. M.; Sutin, N. A Comparison of the Rates of Electron Exchange Reactions of Ammine Complexes of Ruthenium(II) and -(III) with the Predictions of Adiabatic, Outer-sphere Electron Transfer Models. *J. Am. Chem. Soc.* **1979**, *101*, 883−892.
(24) Sutin, N. Theory of Electron Transfer Reactions: Insights and Hindsights. *Progress in Inorganic Chemistry*; John Wiley & Sons, Inc.: NY, 1983; pp 441−498.
(25) Skarda, V.; Cook, M. J.; Lewis, A. P.; McAuliffe, G. S. G.; Thomson, A. J.; Robbins, D. J. Luminescent Metal Complexes. Part 3. Electrochemical Potentials of Ground and Excited States of Ring-Substituted 2,2′-bipyridyl and 1,10-phenanthroline Tris-complexes of Ruthenium. *J. Chem. Soc., Perkin Trans. 2* **1984**, 1309−1311.
(26) Juris, A.; Balzani, V.; Barigelletti, F.; Campagna, S.; Belser, P.; von Zelewsky, A. Ru(II) Polypyridine Complexes: Photophysics, Photochemistry, Eletrochemistry, and Chemiluminescence. *Coord. Chem. Rev.* **1988**, *84*, 85−277.
(27) Al-Rawashdeh, N. A. F.; Chatterjee, S.; Krause, J. A.; Connick, W. B. Ruthenium Bis-diimine Complexes with a Chelating Thioether Ligand: Delineating 1,10-Phenanthrolinyl and 2,2′-Bipyridyl Ligand Substituent Effects. *Inorg. Chem.* **2014**, *53*, 294−307.
(28) Nazeeruddin, M. K.; Zakeeruddin, S. M.; Kalyanasundaram, K. Enhanced Intensities of the Ligand-to-Metal Charge-Transfer Transitions in Ruthenium(III) and Osmium(III) Complexes of Substituted Bipyridines. *J. Phys. Chem.* **1993**, *97*, 9607−9612.
(29) Ronca, E.; De Angelis, F.; Fantacci, S. Time-Dependent Density Functional Theory Modeling of Spin−Orbit Coupling in Ruthenium and Osmium Solar Cell Sensitizers. *J. Phys. Chem. C* **2014**, *118*, 17067−17078.
(30) Mines, G. A.; Roberts, J. A.; Hupp, J. T. Electrochemical and Spectral Probes of Metal/ligand Orbital Mixing in $Ru(NH_3)_4(bpy)^{2+}$ and $Ru(NH_3)_4(phen)^{2+}$. *Inorg. Chem.* **1992**, *31*, 125−128.
(31) Goeltz, J. C.; Benson, E. E.; Kubiak, C. P. Electronic Structural Effects in Self-Exchange Reactions. *J. Phys. Chem. B* **2010**, *114*, 14729−14734.
(32) Goeltz, J. C.; Hanson, C. J.; Kubiak, C. P. Rates of Electron Self-Exchange Reactions between Oxo-Centered Ruthenium Clusters Are Determined by Orbital Overlap. *Inorg. Chem.* **2009**, *48*, 4763−4767.
(33) Maerker, G.; Case, F. H. The Synthesis of Some 4,4′-Disubstituted 2,2′-Bipyridines. *J. Am. Chem. Soc.* **1958**, *80*, 2745−2748.
(34) Doi, T.; Nagamiya, H.; Kokubo, M.; Hirabayashi, K.; Takahashi, T. Synthesis of a Tetrabenzyl-substituted 10-membered Cyclic Diamide. *Tetrahedron* **2002**, *58*, 2957−2963.
(35) Staats, H.; Eggers, F.; Haß, O.; Fahrenkrug, F.; Matthey, J.; Lüning, U.; Lützen, A. Towards Allosteric Receptors—Synthesis of Resorcinarene-Functionalized 2,2′-Bipyridines and Their Metal Complexes. *Eur. J. Org. Chem.* **2009**, *2009*, 4777−4792.
(36) Norris, M. R.; Concepcion, J. J.; Glasson, C. R. K.; Fang, Z.; Lapides, A. M.; Ashford, D. L.; Templeton, J. L.; Meyer, T. J. Synthesis of Phosphonic Acid Derivatized Bipyridine Ligands and Their Ruthenium Complexes. *Inorg. Chem.* **2013**, *52*, 12492−12501.
(37) Ashford, D. L.; Brennaman, M. K.; Brown, R. J.; Keinan, S.; Concepcion, J. J.; Papanikolas, J. M.; Templeton, J. L.; Meyer, T. J. Varying the Electronic Structure of Surface-Bound Ruthenium(II) Polypyridyl Complexes. *Inorg. Chem.* **2015**, *54*, 460−469.
(38) Brady, M. D.; Sampaio, R. N.; Wang, D.; Meyer, T. J.; Meyer, G. J. Dye-Sensitized Hydrobromic Acid Splitting for Hydrogen Solar Fuel Production. *J. Am. Chem. Soc.* **2017**, *139*, 15612−15615.
(39) Troian-Gautier, L.; DiMarco, B. N.; Sampaio, R. N.; Marquard, S. L.; Meyer, G. J. Evidence that $\Delta S^{\ddagger}$ Controls Interfacial Electron Transfer Dynamics from Anatase TiO_2 to Molecular Acceptors. *J. Am. Chem. Soc.* **2018**, *140*, 3019−3029.
(40) Bard, A. J.; Faulkner, L. R. *Electrochemical Methods: Fundamentals and Applications*, 2nd ed.; Wiley: NY, 2001.
(41) Boschloo, G.; Fitzmaurice, D. Spectroelectrochemical Investigation of Surface States in Nanostructured TiO2 Electrodes. *J. Phys. Chem. B* **1999**, *103*, 2228−2231.
(42) Hanson, K.; Losego, M. D.; Kalanyan, B.; Parsons, G. N.; Meyer, T. J. Stabilizing Small Molecules on Metal Oxide Surfaces Using Atomic Layer Deposition. *Nano Lett.* **2013**, *13*, 4802−4809.
(43) Blauch, D. N.; Saveant, J. M. Dynamics of Electron Hopping in Assemblies of Redox Centers. Percolation and Diffusion. *J. Am. Chem. Soc.* **1992**, *114*, 3323−3332.
(44) Blauch, D. N.; Saveant, J. M. Effects of Long-range Electron Transfer on Charge Transport in Static Assemblies of Redox Centers. *J. Phys. Chem.* **1993**, *97*, 6444−6448.
(45) Barbé, C. J.; Arendse, F.; Comte, P.; Jirousek, M.; Lenzmann, F.; Shklover, V.; Grätzel, M. Nanocrystalline Titanium Oxide Electrodes for Photovoltaic Applications. *J. Am. Ceram. Soc.* **1997**, *80*, 3157−3171.
(46) Hansch, C.; Leo, A. *Substituent Constants for Correlation Analysis in Chemistry and Biology*; Wiley: NY, 1979.
(47) Hansch, C.; Leo, A.; Taft, R. W. A Survey of Hammett Substituent Constants and Resonance and Field Parameters. *Chem. Rev.* **1991**, *91*, 165−195.
(48) Farzad, F. Molecular Level Energy and Electron Transfer Processes at Nanocrystalline Titanium Dioxide Interfaces. Ph.D. Dissertation; Johns Hopkins University, 1999.
(49) Ardo, S.; Meyer, G. J. Photodriven Heterogeneous Charge Transfer with Transition-metal Compounds Anchored to TiO_2 Semiconductor Surfaces. *Chem. Soc. Rev.* **2009**, *38*, 115−164.
(50) Ardo, S.; Meyer, G. J. Characterization of Photoinduced Self-Exchange Reactions at Molecule−Semiconductor Interfaces by Transient Polarization Spectroscopy: Lateral Intermolecular Energy and Hole Transfer across Sensitized TiO_2 Thin Films. *J. Am. Chem. Soc.* **2011**, *133*, 15384−15396.
(51) Hu, K.; Robson, K. C.; Beauvilliers, E. E.; Schott, E.; Zarate, X.; Arratia-Perez, R.; Berlinguette, C. P.; Meyer, G. J. Intramolecular and Lateral Intermolecular Hole Transfer at the Sensitized TiO_2 Interface. *J. Am. Chem. Soc.* **2014**, *136*, 1034−1046.
(52) Anslyn, E. V.; Dougherty, D. A. *Modern Physical Organic Chemistry*; University Science: Sausalito, CA, 2006.
(53) Charton, M. Nature of the ortho effect. II. Composition of the Taft steric parameters. *J. Am. Chem. Soc.* **1969**, *91*, 615−618.
(54) Charton, M. Steric Effects. I. Esterification and Acid-catalyzed Hydrolysis of Esters. *J. Am. Chem. Soc.* **1975**, *97*, 1552−1556.
(55) Timperley, C. M.; White, W. E. The Steric and Electronic Effects of Aliphatic Fluoroalkyl Groups. *J. Fluorine Chem.* **2003**, *123*, 65−70.
(56) Gutzler, R.; Ivasenko, O.; Fu, C.; Brusso, J. L.; Rosei, F.; Perepichka, D. F. Halogen Bonds as Stabilizing Interactions in a Chiral Self-assembled Molecular Monolayer. *Chem. Commun.* **2011**, *47*, 9453−9455.
(57) Metrangolo, P.; Franck, M.; Tullio, P.; Giuseppe, R.; Giancarlo, T. Halogen Bonding in Supramolecular Chemistry. *Angew. Chem., Int. Ed.* **2008**, *47*, 6114−6127.
(58) Kobori, Y.; Yago, T.; Akiyama, K.; Tero-Kubota, S.; Sato, H.; Hirata, F.; Norris, J. R. Superexchange Electron Tunneling Mediated by Solvent Molecules: Pulsed Electron Paramagnetic Resonance Study on Electronic Coupling in Solvent-Separated Radical Ion Pairs. *J. Phys. Chem. B* **2004**, *108*, 10226−10240.
(59) Murata, S.; Matsuzaki, S. Y.; Tachiya, M. Transient Effect in Fluorescence Quenching by Electron Transfer. 2. Determination of the Rate Parameters Involved in the Marcus Equation. *J. Phys. Chem.* **1995**, *99*, 5354−5358.

DOI: 10.1021/acs.jpcc.8b05281
J. Phys. Chem. C 2018, 122, 19385−19394

(60) Tavernier, H. L.; Kalashnikov, M. M.; Fayer, M. D. Photoinduced Intermolecular Electron Transfer in Complex Liquids: Experiment and Theory. *J. Chem. Phys.* **2000**, *113*, 10191−10201.
(61) Miller, J. R.; Beitz, J. V.; Huddleston, R. K. Effect of Free Energy on Rates of Electron Transfer between molecules. *J. Am. Chem. Soc.* **1984**, *106*, 5057−5068.
(62) Yonemoto, E. H.; Saupe, G. B.; Schmehl, R. H.; Hubig, S. M.; Riley, R. L.; Iverson, B. L.; Mallouk, T. E. Electron-Transfer Reactions of Ruthenium Trisbipyridyl-Viologen Donor-Acceptor Molecules: Comparison of the Distance Dependence of Electron Transfer-Rates in the Normal and Marcus Inverted Regions. *J. Am. Chem. Soc.* **1994**, *116*, 4786−4795.

DOI: 10.1021/acs.jpcc.8b05281
J. Phys. Chem. C 2018, 122, 19385−19394